Direct evidence for the ring opening of monosaccharide anions in the gas phase: photodissociation of aldohexoses and aldohexoses derived from disaccharides using variable-wavelength infrared irradiation in the carbonyl stretch region

Darin J. Brown [a,†], Sarah E. Stefan [b,†,‡], Giel Berden [c], Jeffrey D. Steill [c,§], Jos Oomens [c,d], John R. Eyler [b], Brad Bendiak [a,*]

[a] Department of Cell and Developmental Biology and Program in Structural Biology and Biophysics, University of Colorado Denver, Anschutz Medical Campus, Aurora, CO 80045, United States
[b] Department of Chemistry, University of Florida, Gainesville, FL 32611-7200, United States
[c] FOM Institute for Plasma Physics Rijnhuizen, Molecular Dynamics Group, Edisonbaan 14, 3439 MN Nieuwegein, The Netherlands
[d] van't Hoff Institute for Molecular Sciences, University of Amsterdam, Science Park 904, 1098XH Amsterdam, The Netherlands

ARTICLE INFO

ABSTRACT

All eight D-aldohexoses and aldohexoses derived from the non-reducing end of disaccharides were investigated by variable-wavelength infrared multiple-photon dissociation (IRMPD) as anions in the negative-ion mode. Spectroscopic evidence supports the existence of a relatively abundant open-chain configuration of the anions in the gas phase, based on the observation of a significant carbonyl absorption band near 1710 cm^{-1}. The abundance of the open-chain configuration of the aldohexose anions was approximately 1000-fold or greater than that of the neutral sugars in aqueous solution. This provides an explanation as to why it has not been possible to discriminate the anomeric configuration of aldohexose anions in the gas phase when derived from the non-reducing sugar of a disaccharide. Evidence from photodissociation spectra also indicates that the different aldohexoses yield product ions with maximal abundances at different wavelengths, and that the carbonyl stretch region is useful for differentiation of sugar stereochemistries. Quantum-chemical calculations indicate relatively low energy barriers to intramolecular proton transfer between hydroxyl groups and adjacent alkoxy sites located on open-chain sugar anions, suggesting that an ensemble of alkoxy charge locations contributes to their observed photodissociation spectra. Ring opening of monosaccharide anions and interconversion among configurations is an inherent property of the ions themselves and occurs in vacuo independent of solvent participation.

1. Introduction

Mass spectrometry has long been an important tool for the analysis of complex carbohydrates. Tandem techniques have been developed for multiple stages of isolation and dissociation that include ion traps,[1,2] concatenated quadrupole designs,[3] time-of-flight instruments,[4,5] Fourier-transform ion cyclotron resonance (FTICR) instruments[6] or combinations thereof. This has enabled precursor ions of oligosaccharides to be broken down and their fragments to be isolated in consecutive steps. As many steps as technically possible are wanted, because evidence is needed for the stereochemistries, anomeric configurations, ring forms, linkage positions and possible hydroxyl group substitutions of monosaccharides that make up larger structures. The unimolecular dissociation of larger oligosaccharides usually proceeds via sets of substructures, such as trisaccharides, disaccharides, monosaccharides and other substructures representing portions of these ions derived from cross-ring cleavages. Disaccharides represent the smallest substructures that still contain a glycosidic linkage between two sugars. Their dissociation has been investigated, and characteristic product ions derived from them have been reported, both in the positive- and negative-ion modes.[7–21] At least two of these product ions have been shown to have potential for identification of the stereochemistries and anomeric

---

* Corresponding author. Tel.: +1 303 724 3453.
E-mail address: brad.bendiak@ucdenver.edu (B. Bendiak).
† These authors contributed equally to investigations.
‡ Present address: Department of Natural Sciences, Florida State College at Jacksonville, Jacksonville, FL 32256, United States.
§ Present address: Sandia/California, 7011 East Avenue, Livermore, CA 94551, United States.

configurations of the molecules. They are the glycosyl-glycolalde-hydes[14,15,22] and the monosaccharides (in the negative-ion mode, m/z 221 and 179, respectively, and in the positive-ion mode with lithium, for example, the m/z 229 and 187 ions, respectively). These ions contain the minimum number of stereochemical centers to potentially identify the nature of each sugar derived from a completely unknown disaccharide.

Monosaccharides are the fundamental building blocks of larger molecules, and thus it is crucial to be able to clearly determine the stereochemistry of their structures in the gas phase. They are frequently observed as dissociation products at different stages of multiple tandem mass spectrometry experiments (MS^n) as primary, secondary, or tertiary product ions derived from larger oligosaccharides. In the positive-ion mode, four of the 8 possible aldohexoses were shown to be differentiated as either lead[23] or ammonium[24] adducts. In the negative-ion mode, it has been reported that their dissociation patterns using collision-induced dissociation (CID), at least for some of the monosaccharides, are too similar to confidently assign their stereochemistry.[15] Moreover, assignment of the anomeric configuration of a monosaccharide product ion derived from a disaccharide has not been possible. Evidence in the negative-ion mode has shown that the monosaccharide anions derived from the non-reducing sugar of disaccharides having either an α or β linkage yield essentially identical dissociation patterns using CID.[15] These disaccharides had been ^{18}O-labeled on the reducing sugar to mass-discriminate the origins of monosaccharides from either side of the glycosidic linkage. It has been proposed that the reason for the similarity of dissociation patterns for monosaccharides derived from either an α or β linkage might be due to the ring opening of the sugar ions upon their acquisition of enough internal energy to reach the threshold for unimolecular dissociation.[15,13,7,25,26] Proposed mechanisms of monosaccharide dissociation have suggested retro-aldol type rearrangements that proceed through an open-chain form of the sugar.[26,27,7,17] However, direct evidence for the open-chain forms of the ions in the gas phase has not been reported. The structures of monosaccharide ions in the gas phase are still far from clear, partly because there are few methods to experimentally evaluate what might be multiple configurations and/or conformations of the ions.

In solution, six distinct structures of monosaccharides have been observed, with proportions for D-glucose shown in Scheme 1. Notably relevant to the present report is that the open-chain (carbonyl) form in aqueous solution is present in extremely low concentrations, which has been confirmed by multiple physical techniques. These include (1) NMR of 1-^{13}C-D-glucose (0.002%),[28] (2) mutarotation kinetics (0.0026%),[29] (3) the dichroic extinction coefficient (0.002%)[30] and (4) reaction kinetics with urazole (0.0014%).[31] Also worthy of note is that heating an aqueous solution from 27 °C to 82 °C resulted in an approximately 10-fold increase in the carbonyl form, as evaluated by NMR spectroscopy.[28] Although the carbonyl form had been suspected in solution for over a century based on reactivities[32] and enolization[33] of sugars,

spectroscopic observation and quantitation of the multiple forms shown in Scheme 1 was not forthcoming for many years.

All of the above evidence and hypotheses prompted two questions. First, do the equilibrium ratios of monosaccharide configurations (Scheme 1) necessarily bear any similarity to those of a negatively charged ion in the gas phase, and how do these ratios change upon acquiring enough internal energy to approach a dissociation threshold? Second, if similar ratios do exist in the gas phase, could enough open-chain form exist to then kinetically explain previous observations concerning their patterns of dissociation? For example, in aqueous solution, tens of minutes to a few hours are typically required for sugars to reach an equilibrium optical rotation through the open-chain structure shown in Scheme 1,[34] yet unimolecular dissociation events in mass spectrometers typically occur in the range of microseconds to milliseconds. Even at high pH (as high as pH 13.7) in aqueous solution, where anionic species of sugars are present, ^{13}C NMR experiments have shown that the α- and β-pyranose forms of glucose are highly predominant, and are stable for a significantly longer time period than a typical free-induction decay period of 1–2 s.[35,36] Notably, open-chain forms were not observed at high pH but may have been present in negligible quantities.

Bearing these issues in mind, experiments were undertaken to investigate the structures of hexose anions in the gas phase using variable-wavelength infrared multiple-photon dissociation (IRMPD), a technique that can evaluate the presence of various functional groups found in gas-phase ions based on their vibrational spectroscopy. It has two key advantages over collision-induced dissociation. First, CID imparts a broad range of energies to ions, depending on the orientation and geometry of collisions (the impact parameter). Calculations have indicated that energies ranging from the equivalent of a UV photon to nearly zero are imparted to ions.[37] This is the spectroscopic equivalent of using the entire bandwidth of a tungsten filament as a source, then expecting to observe fine differences in dissociation of isomeric monosaccharides after absorption over a wide range of photon energies. Scanning with a narrow linewidth source enables dissociation of ions to be assessed as a function of wavelength, which can be plotted in a second dimension to correlate their absorption and dissociation patterns.[20,38] Spectra can be practically assessed in the UV, visible and infrared ranges of the electromagnetic spectrum,[38–46] and more recently as a function of the pulse shape of laser sources.[47,48] Second, photodissociation is advantageous over CID in FTICR mass spectrometers where ions are investigated under high-vacuum conditions, as CID temporarily involves raising the pressure. The time needed for pump-down before signal detection lowers the duty cycle and significant losses occur due to product ion scattering.[49]

Previously, in the condensed phase (mineral oil, Nujol, or water), the presence of a carbonyl absorbance for aldohexoses in infrared spectra has been either negligible or unobservable[50–52] in keeping with the low abundance of the open-chain form found by the other physical methods discussed above. Herein we report for the first time the direct observation of the absorbance of the carbonyl C=O stretch group for the negative ions of all eight aldohexoses. It was observed in much higher abundance than previously found in condensed-phase IR spectra. Differences in dissociation spectra of the aldohexoses were also observed in the carbonyl stretch region, with wavelength maxima for product-ion abundances that varied from sugar to sugar. Theoretical calculations indicate that the negative charge may be located at different alkoxy positions on the open-chain form of D-glucose, and that intramolecular proton transfer can occur through transition states having a relatively low energy barrier. This may explain, at least in part, some of the wavelength-dependent differences in dissociation observed among sugars.
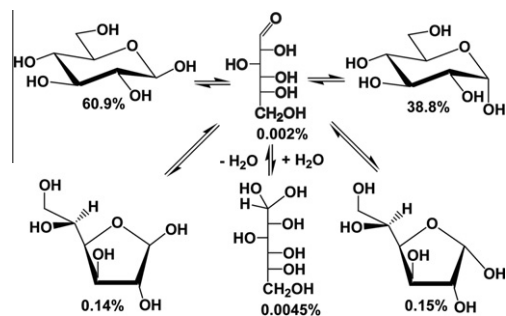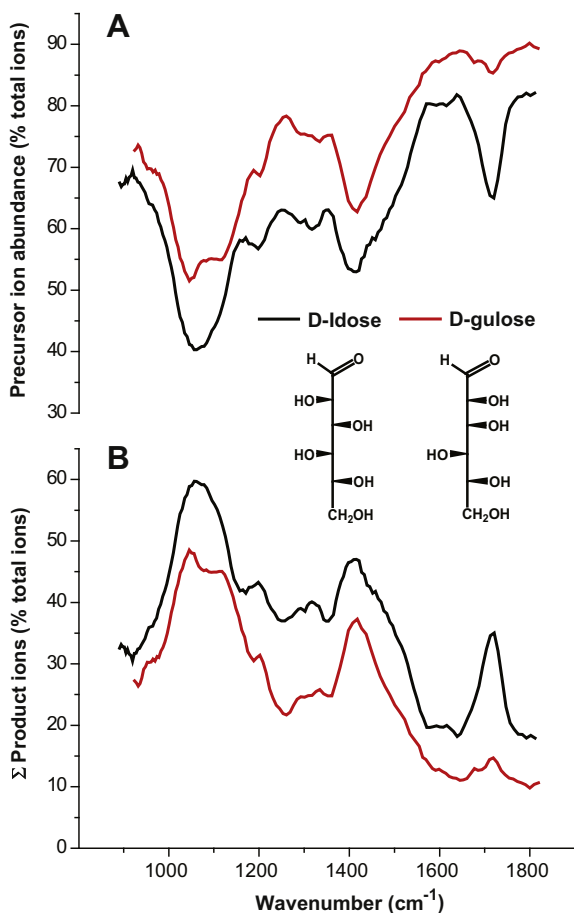

Scheme 1.

2. Results and discussion

2.1. Evidence for the open-chain configuration of negative ions of aldohexoses in the gas phase

The infrared photodissociation spectra of D-idose and D-gulose over the spectral range from 5.5 to 11.4 μm (880–1820 cm^{-1}), are shown in Figure 1. The spectra represent (A) the decrease in the abundance of the precursor (m/z 179) ion (upper pair) and (B) the total sum of the product ions (lower pair), as a function of wavelength. A significant peak was observed at wavelengths near 5.8 μm (1700 cm^{-1}), which is the classic region of the C=O stretch. The highest absorption was measured over the spectral region from about 900 to about 1430 cm^{-1}, which is the classic 'fingerprint region' of hexose infrared spectra that includes C–H and O–H bend, C–O and C–C stretch frequencies, and H–C–O, C–C–H and C–O–H deformations, among others.[51,52] These two specific sugars were selected for Figure 1 as they represent the extremes that were observed in absorbance in the carbonyl region (1650–1750 cm^{-1}). The 'dip' in the abundance of the precursor ion for all the aldohexoses ranged from a minimum of about 3–4% for gulose to about 17% for idose, at the power levels and pulse structure used in these experiments. Comparisons to direct absorption IR spectra in condensed phases would be expected to be somewhat
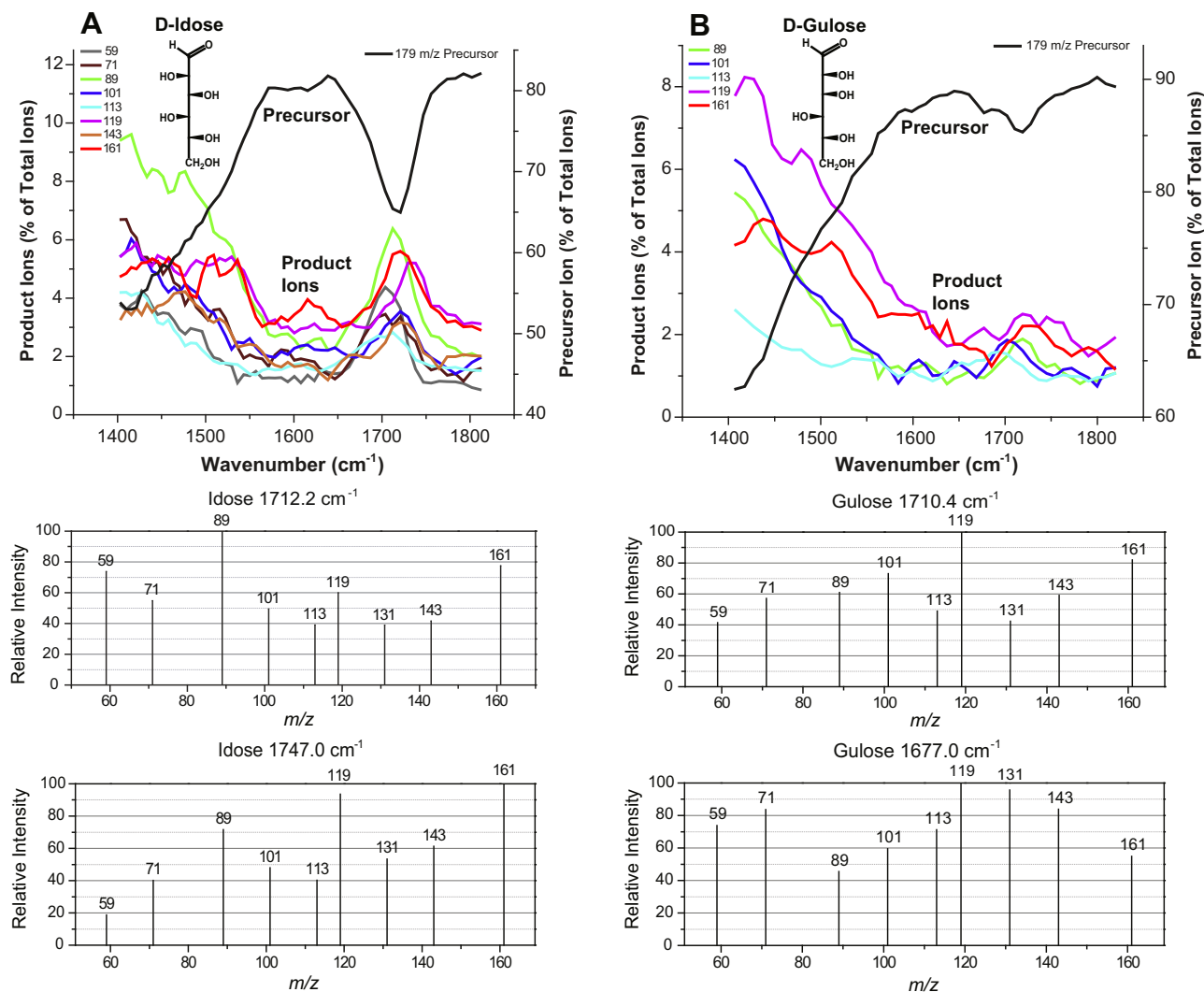
different for the following reasons. First, infrared photodissociation is an action spectrum dependent both upon absorption at specific wavelengths and unimolecular dissociation events at internal energy levels above some threshold required for fragmentation. Second, the presence of a negative charge, possibly located at different alkoxy positions when considering an entire population of ions, would be expected to affect absorption frequencies as compared to neutral molecules. The charge location potentially alters the equilibrium populations of configurations and conformations of ions through internal hydrogen bonding of hydroxyl groups to neighboring alkoxy positions. The infrared photodissociation spectra of alkali metal adducts of hexoses, disaccharides and methyl glycosides in the positive-ion mode (Na$^+$, Li$^+$ and Rb$^+$)[20,38,46,53] have been previously measured. These adducts showed a major absorption over the region from about 900 to 1450 cm^{-1} and at well-defined hydroxyl stretch frequencies in the 3200 to 4000 cm^{-1} region. In the negative-ion mode in this report, a clear dip was observed in the precursor ion abundance upon irradiation at the carbonyl frequency for all aldohexose anions, as detailed below.

2.2. Photodissociation spectra of the open-chain forms of aldohexoses in the gas phase and features of their infrared wavelength-dependence near the carbonyl stretch region

Photodissociation experiments were carried out on all the aldohexoses as anions. Spectral regions spanning the carbonyl stretching band are presented in Figures 2–5. The carbonyl stretch region appears to range from about 1650 to about 1770 cm^{-1}, possibly wider, depending on the isomer. Spectra acquired in this region resulted from unimolecular dissociation of a selected subpopulation of ions having a C=O stretch, or possibly multiple open-chain states, depending on the real possibility of different negative charge locations (alkoxy sites) on these ions. The structures shown in each figure were therefore drawn in the open-chain form. In Figure 2A, more details of the wavelength dependence of the photodissociation of idose are shown. Other than the observed decrease in the precursor ion abundance in the carbonyl region, the appearance and relative abundance of several product ions as a function of wavelength is presented. The structures of product ions have been proposed previously for hexoses, with neutral losses in multiples of m/z 30 suggested to be smaller sugars such as the tetroses or glyceraldehyde (m/z 119, and 89, respectively) or epoxide hemiacetals, while other product ions are believed to be derived by mechanisms that additionally involve dehydration with formation of double bonds.[25] Note that the precursor ion showed a diminished intensity with a minimum near 1715 cm^{-1} (Fig. 2A). However, the wavelengths for the maximal abundance of specific product ions in this region were not identical to that observed for the decrease of the m/z 179 precursor ion. For example, ions of m/z 89 and 59 showed maximal abundance near a wavelength of 1710 cm^{-1}, whereas maxima shifted to near 1720 cm^{-1} for the 161, 143, and 101 product ions, and to near 1730 for the m/z 119 ion. Notably, several product ions shifted in relative abundance as a function of wavelength, whereby their intensities crossed over at specific wavelengths. For example, mass spectra accumulated at two wavelengths (1712 and 1747 cm^{-1}) are presented at the bottom of Figure 2A. Note that the ratios of the m/z 59 to 71 product ions changed markedly, as did the ratio of the 89 to 119 product ions. As shown in the top spectral plot in Figure 2A, between the wavelengths of about 1660–1730 cm^{-1}, the m/z 89 ion was of greater relative abundance than the m/z 119 ion, but at higher cm^{-1} values than 1730, the m/z 119 ion was more abundant. Similarly the m/z 59 ion was more abundant than the m/z 71 ion between wavelengths of about 1675–1725 cm^{-1}, yet the m/z 71 ion predominated at higher cm^{-1} values. These selected

Figure 1. A comparison of photodissociation of D-idose and D-gulose anions (precursor m/z 179) over the wavelength range from 880 to 1820 cm^{-1}. Shown in panel A is the diminishment of the precursor ion abundance as a function of wavelength, and in panel B is the increase in abundance of summed product ions. Full plots are shown to illustrate the relative photodissociation that resulted from absorbance in the carbonyl region (1650–1750 cm^{-1}) as compared to the 'fingerprint region' (900–1450 cm^{-1}) reported in condensed-phase IR spectra.[50–52]

Figure 2. A comparison of photodissociation of the C-2 epimers D-idose and D-gulose, showing the 1400–1820 cm^{-1} wavelength region of the spectrum, with individual product ion abundances as well as the precursor ion abundance plotted as a function of wavelength in the top plots of A and B. The bottom two plots in each column are two mass spectra obtained for each sugar precursor ion (m/z 179); one was the closest experimental wavelength point to 1710 cm^{-1} used during the free-electron laser scan, and the other was selected at a nearby wavelength that yielded a significantly different ratio of product ions. The legend for the abundance of specific product ions is shown in colors with each wavelength plot in A and B.

examples with the idose anion illustrate that unique wavelength-dependent changes in fragmentation spectra occur in the region of the carbonyl stretch absorbance. Although not understood in detail, this behavior can be accounted for by the underlying multiple-photon excitation process. As the precursor ion fragments into product ions, the various dissociation channels have different thresholds, and as the number of photons required to reach a specific threshold increases, the effects of anharmonicity on the apparent band center become more pronounced. A striking manifestation of this effect has been described,[54] and methods to theoretically model these processes have also been reported.[55,56]

In Figure 2B, the photodissociation spectrum of D-gulose is shown over the same spectral region. The overall diminution of the precursor ion abundance (3–4% dip) was significantly less than that observed for idose (Fig. 2A). These two sugars are epimers at C-2; thus the asymmetry of C-2 significantly affected photodissociation events. Note that not as many product ions were plotted in Figure 2B as compared to 2A; for purposes of clarity, some of the ions that did not significantly increase in abundance over the 1650–1770 cm^{-1} spectral region were not presented (i.e., their profiles remained relatively flat over this portion of the spectrum).

Potential reasons for this are discussed below. Other product ions increased in relative abundance in this region and most showed different wavelength maxima and relative abundances as compared to idose (compare Fig. 2A and B). For example, wavelength maxima for the abundances of the m/z 161, 101 and 89 product ions were observed for idose near 1720, 1720, and 1710 cm^{-1} but for gulose near 1730, 1700, and 1720 cm^{-1}, respectively. The most abundant product ion from 1400–1500 and 1675–1725 cm^{-1} for idose was the m/z 89 ion, the m/z 119 ion being less abundant over these spectral ranges (Fig. 2A). However, for gulose, the m/z 119 ion was more abundant than the m/z 89 ion over the entire spectral range from 1400 to 1820 cm^{-1}. The ratios of product ions in mass spectra for gulose (Fig. 2B, bottom two mass spectra) were highly wavelength dependent in the carbonyl stretch region. For instance, an examination of the m/z 59:89 or 131:161 ratios revealed a shift from significantly less than 1 to significantly greater than 1 in comparing the spectra at 1710 and 1677 cm^{-1}, respectively. It is also worth noting that the mass spectra of all aldohexoses are shown in this and in succeeding figures near the wavelength of 1710 cm^{-1}; slight differences in the specific wavelengths selected were due to differences in the
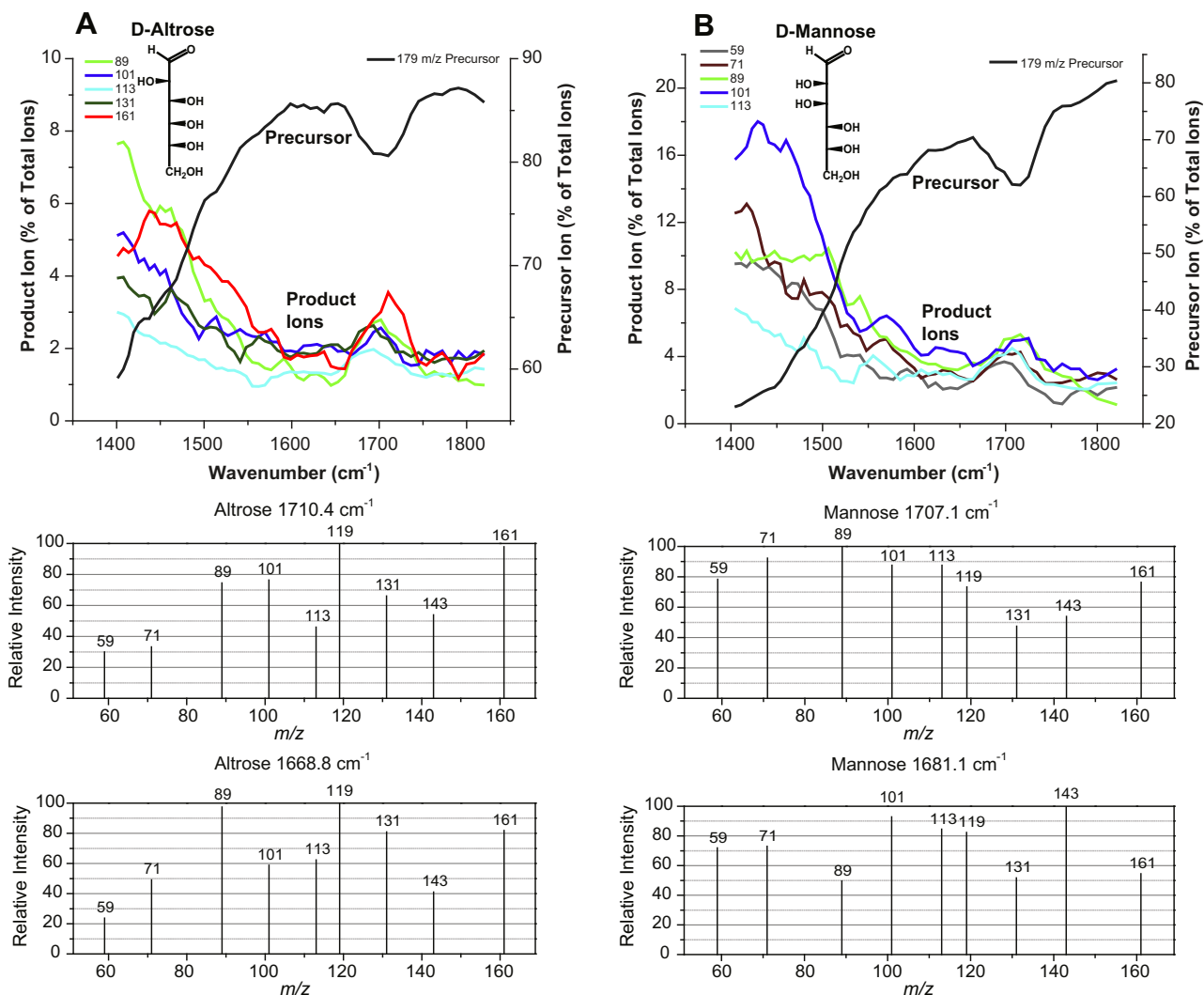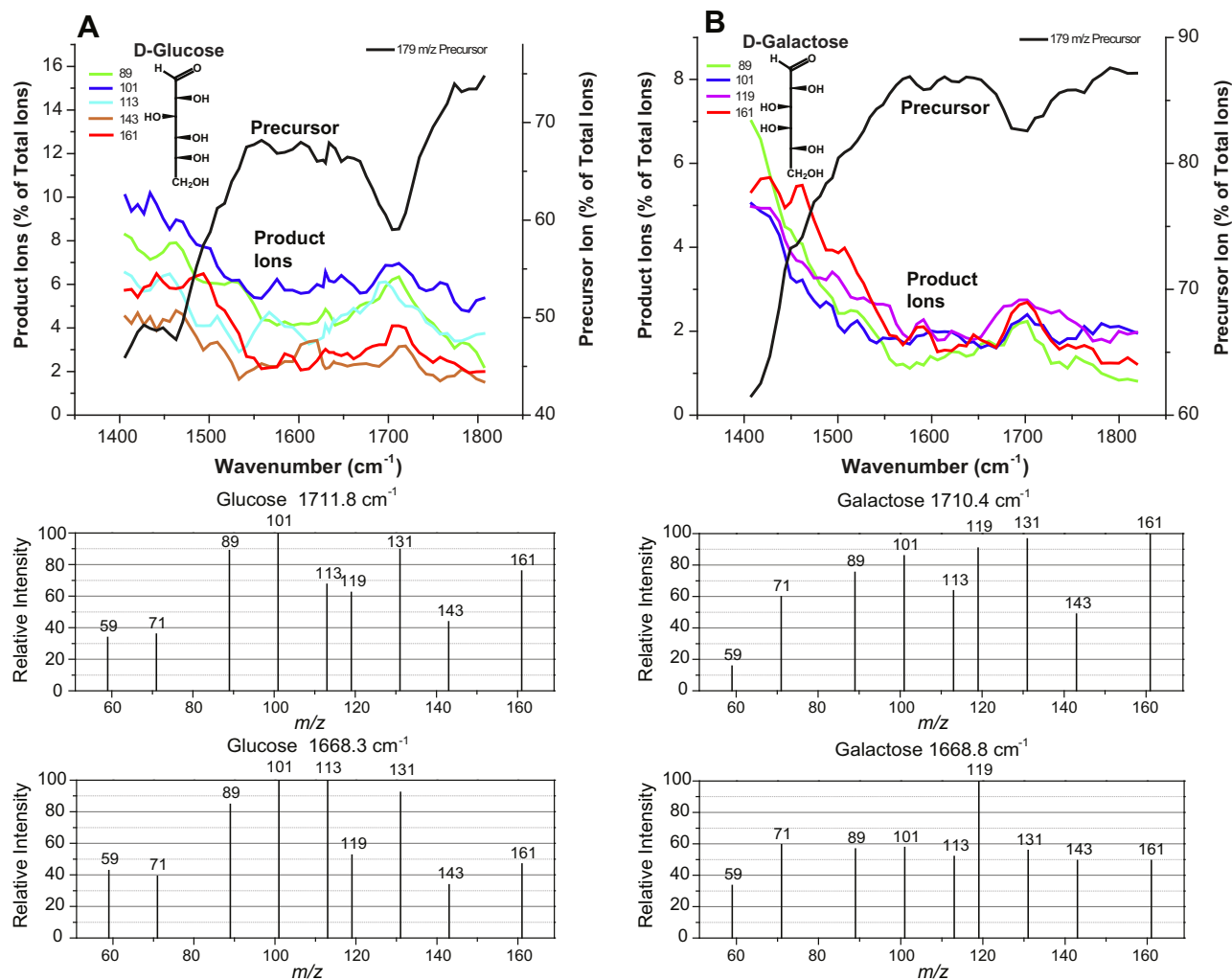
Figure 3. Photodissociation of the C-3 epimers D-altrose and D-mannose over the 1400–1820 cm^{-1} wavelength range. Individual product ion abundances as well as the precursor ion abundance were plotted as a function of wavelength over the region, in the top plots of A and B. The bottom plots in each column are mass spectra obtained for each sugar negative-ion precursor ion (m/z 179). One was the closest experimental point to a wavelength of 1710 cm^{-1} used during the free-electron laser scan, and the other was selected at a nearby wavelength having a significantly different ratio of product ions. Relevant product ion abundances are shown in colors indicated by the legend in the upper left corner.

precise incrementation of the wavelengths from the free-electron laser over the scanning range. In the case of idose and gulose (Fig. 2), the comparison between idose at 1712 cm^{-1} and gulose at 1710 cm^{-1} showed different base-product ions and significantly different product ion ratios. Note that a 2–3 cm^{-1} difference in the center of the irradiation wavelength did not result in a marked change in mass spectral product ion ratios for any of the individual sugars; changes with wavelength were somewhat more gradual as shown in Figure 2A and B. Hence large differences in the product ion ratios of different aldohexoses irradiated near 1710 cm^{-1}, as shown in Figure 2 and some additional figures, result from structural differences among the open-chain forms.

In Figure 3, a comparison of the two C-3 epimers, D-altrose and D-mannose, is shown over the wavelength region containing the carbonyl stretch, and mass spectra at selected wavelengths are shown in the bottom panels. The dip in the abundance of the precursor (m/z 179) ion near 1710 cm^{-1} was about 6–10% of the precursor ion abundance. Like the comparison between the epimers of gulose and idose, differences were observed in the abundance and wavelength maxima for specific product ions, indicating that the asymmetry at C-3 also has an effect on

photodissociation in the carbonyl stretch region. Mass spectra (bottom panels, Figure 3) reflect some of the significant changes that occur in dissociation with wavelength over this region. For example, with altrose, ratios of m/z 89/101 and 131/161 changed in comparing spectra taken from wavelengths of 1668.8 and 1710.4 cm^{-1}. With mannose, the relative abundances of the product ion pairs 59:89 and 143:161 reverse in comparing spectra from wavelengths of 1681.1 and 1707.1 cm^{-1}. Also, in comparing the spectra of the two hexoses at 1710.4 and 1707.1 cm^{-1}, it was evident that base-product ions (m/z 119 and 89) were different and large differences were observed in the abundances of the m/z 59, 71 and 113 product ions.

In Figure 4, the photodissociation spectra of two C-4 epimers, D-glucose and D-galactose, are presented over the carbonyl stretch region. These two sugars, in particular, are commonly found in many biological systems and are not possible to differentiate in the negative-ion mode using collision-induced dissociation.[15] Similar to the other comparisons, the precursor ion was depleted over the carbonyl stretch region by about 5–10%, and an increase in specific product ions was evident. Notably, ion ratios varied with wavelength in comparing mass spectra in the bottom panels. With

Figure 4. Photodissociation spectra of the 4-epimers D-glucose and D-galactose over the 1400–1820 cm^{-1} wavelength region. Individual product ion abundances and the precursor ion abundance are plotted as a function of wavelength in the top plots of A and B. The bottom plots in each column are mass spectra obtained for each sugar precursor negative ion (m/z 179). One was the closest experimental wavelength point to 1710 cm^{-1} used in the free-electron laser scan, and the other was selected at a nearby wavelength that gave a significantly different ratio of product ions. Appropriate key product ion abundances are indicated in colors in the legend.

glucose, for example (Fig. 4A), the m/z 113 product ion increased, and the m/z 161 ion decreased relative to several other ions in comparing photodissociation wavelengths of 1711.8 with 1668.3 cm^{-1}, respectively. With galactose, however (Fig. 4B), the most dramatic changes in comparing mass spectra from similar wavelengths to those of glucose (the two bottom panels) were the abundances of the m/z 131 and 161 product ions. Relative abundances of other ions, however, were also different between the two sugars (compare mass spectra at either the m/z 1711.8:1710.4 or 1668.3:1668.8 in Fig. 4A and B)

In Figure 5, the infrared wavelength-dependent photodissociation spectra of the remaining two aldohexoses, D-allose and D-talose, are shown. In this case, these two sugars vary in the stereochemistry at C-2, C-3 and C-4. As with the other experiments and comparisons (Figs. 2–4), these sugars revealed a depletion of the precursor ion abundance and the appearance of more abundant product ions in the region covering the carbonyl stretch. The mass spectra in the bottom two panels for Figure 5A and B showed differences in the abundances of specific product ions that varied with wavelength for a single sugar, and between sugars at wavelengths near 1710 cm^{-1}.

In Figure 6, variation of the abundances of certain key product ions from different aldohexoses with wavelength is presented over

the carbonyl stretch region. The m/z 161 product ion (Fig. 6A) varied in maximal abundance with wavelength from near 1700 cm^{-1} (for galactose) to near 1735 cm^{-1} (for mannose). The m/z 101 product ion (Fig. 6B) varied in wavelength maxima between 1710 cm^{-1} (for allose) and 1730 cm^{-1} (for mannose). As indicated in Figure 6C, the m/z 89 product ion ranged in wavelength maxima between 1690 cm^{-1} (for allose) to near 1720 cm^{-1} (for mannose). These comparisons demonstrate that unique features of the photodissociation of gas-phase state(s) of specific hexose anions can be probed by varying infrared wavelengths over the carbonyl stretch region, giving rise to product ions having different wavelength maxima.

Taken together, data from wavelength-dependent photodissociation of all the aldohexoses indicate that a significant proportion of the molecular ions in the gas phase exist in the open-chain carbonyl form. The proportion of open-chain form(s) is far greater than previously observed in experiments performed with condensed-phase samples (solid or dissolved in water). Different sugars are prone to relatively marked variations in their patterns of photodissociation versus wavelength over the carbonyl stretch region. Potential reasons for these observations are discussed in further detail below. Approximate estimates of the relative proportion of the open-chain to cyclic configurations are anywhere from
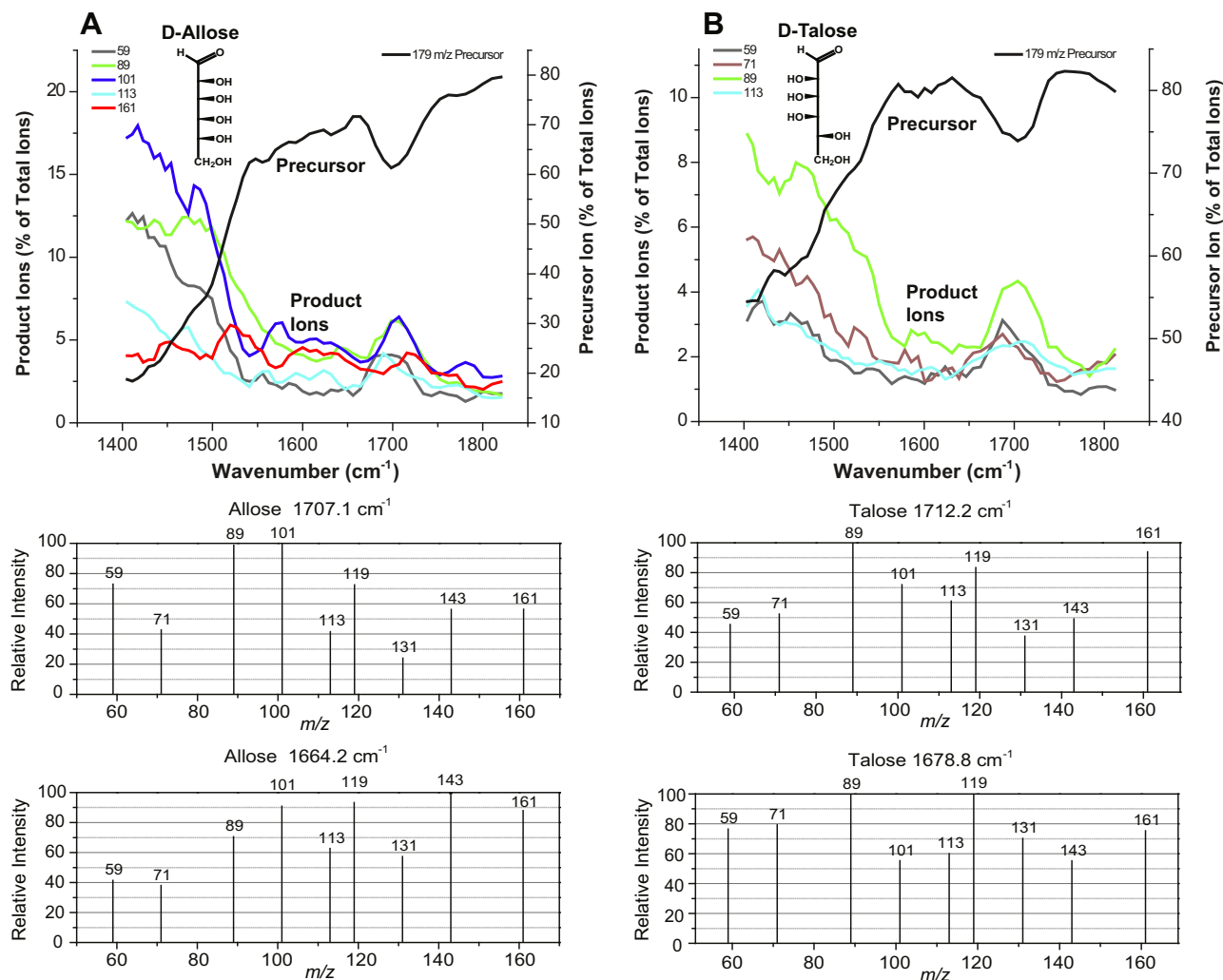
Figure 5. Photodissociation spectra of D-allose and D-talose over the 1400–1820 cm^{-1} wavelength region. Individual product ion abundances and the precursor ion abundance are plotted as a function of wavelength in the top plots of A and B. The bottom plots in each column are mass spectra obtained for each sugar precursor negative ion (m/z 179). One was the closest experimental wavelength point to 1710 cm^{-1} used in the free-electron laser scan, and the other was selected at a nearby wavelength that yielded a significantly different ratio of product ions. Relevant product ion abundances are indicated in colors in the legend.

1% to 20%. This is based on the relative absorbance of the carbonyl stretch to the 'fingerprint' region (900–1450 cm^{-1}) observed in liquid phase for glyceraldehyde, a molecule incapable of cyclization.[57] At less than a 1% ratio of open-chain/cyclic configurations, we would anticipate the carbonyl absorbance 'dip' to be too low to be observed in our experiments. Nonetheless, these approximate boundaries on the relative proportion of the open-chain form are much higher than those observed in aqueous solution (2×10^{-5}), on the order of 10^3–10^4 higher. This is in keeping with the unobservable carbonyl stretch in condensed-phase infrared spectroscopy of aldohexoses[50–52] and a variety of other physical measurements in solution.[28–31]

2.3. Evidence for the open-chain form of monosaccharide product ions derived from the non-reducing sugar of disaccharides having either anomeric configuration

Evidence from previous studies[7–15] has indicated that a monosaccharide product ion (m/z 179) is frequently derived from various disaccharides following CID. However, upon isolation of this ion the anomeric configuration of the sugar cannot be ascertained directly from its dissociation pattern,[15] as illustrated

in Scheme 2. It has been proposed by various investigators[15,13,7,25,26] that a monosaccharide anion rapidly interconverts between anomeric forms in the gas phase via the open-chain carbonyl form. Interconversion could potentially occur on the same time scale as further isolation and dissociation events. This strongly suggested that monosaccharide anions derived from the (original) non-reducing sugar of a disaccharide could be in rapid equilibrium with the open-chain form and that perhaps their carbonyl stretch frequencies could be detected in the gas phase.

An experiment to test this possibility is presented in Figure 7. Infrared photodissociation spectra of the monosaccharide product ion (m/z 179) derived from the non-reducing sugar of two disaccharides differing in their anomeric configuration are shown. The disaccharides, α-D-Glcp-(1→2)-D-Glc and β-D-Glcp-(1→2)-D-Glc were ^{18}O-labeled on the carbonyl group of the reducing sugar so that the monosaccharide product ion, including the oxygen derived from the glycosidic linkage, could be mass-discriminated from the monosaccharide product ion potentially derived from the reducing hexose (Scheme 2). The two spectra of the glucose product ions derived from either anomeric configuration were nearly identical. Both showed a comparable increase in abundance of product ions in the region of the absorbance of the carbonyl
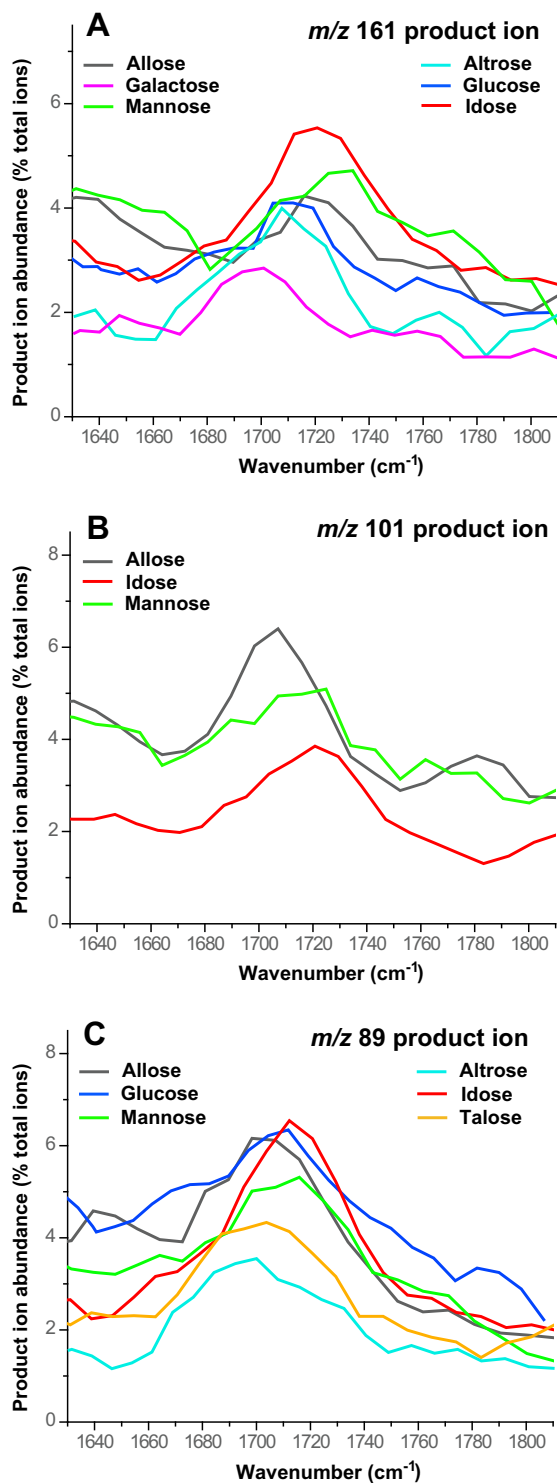
Figure 6. A comparison of wavelength optima observed for the abundances of specific product ions derived from different sugars over the carbonyl stretch region. Shown are the product ion abundances generated as a function of wavelength from 1630 to 1810 cm⁻¹. The profiles are shown for (A) the *m/z* 161 product anion, (B) the *m/z* 101 product anion, and (C) the *m/z* 89 anion. Not all the aldohexose profiles are plotted; for some of the sugars, plots of the above ions were nearly horizontal across this region and were therefore not included. Those most illustrative of differences in wavelength maxima among the sugars were presented, each with a different color indicated in the legend.
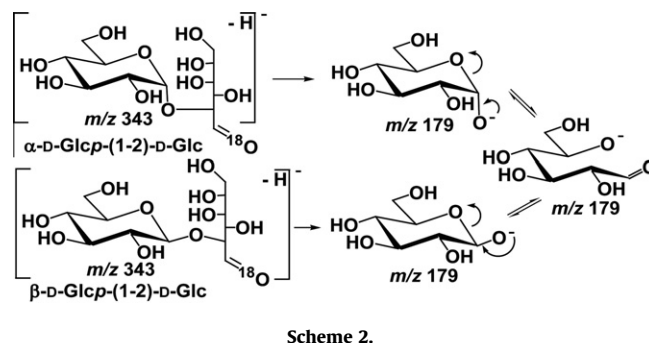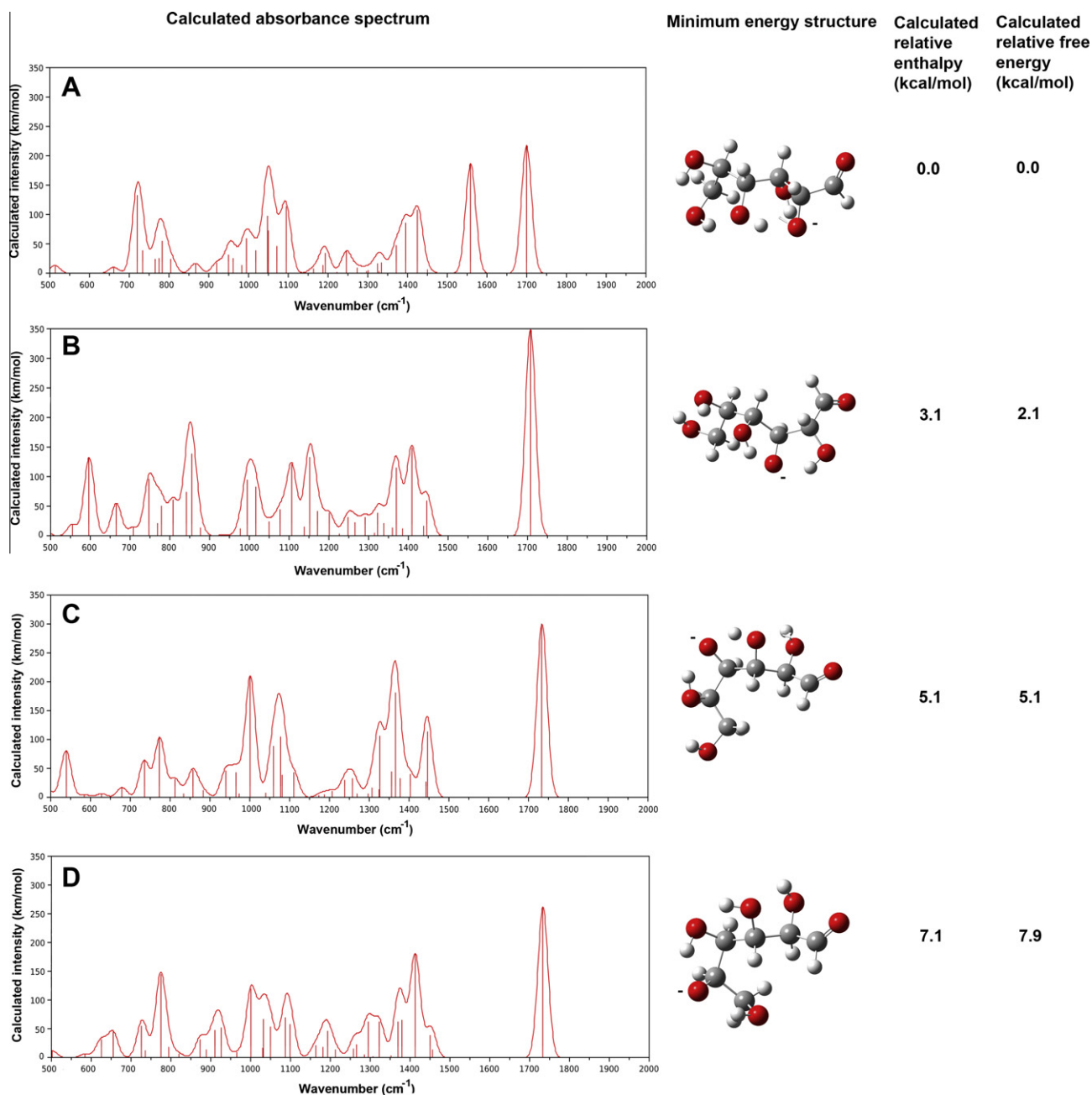

Scheme 2.
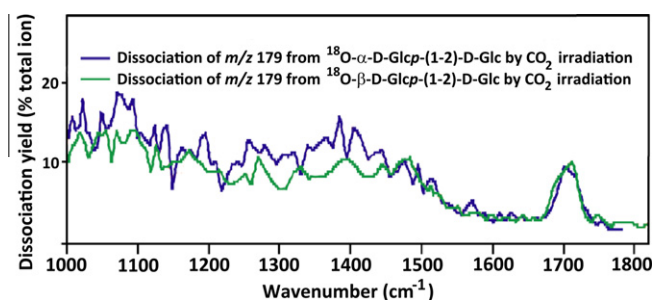
Figure 7. Variable-wavelength infrared multiple-photon dissociation spectra of isolated monosaccharide (*m/z* 179) anions derived from the non-reducing sugar of disaccharide (*m/z* 343) ions that were ¹⁸O-labeled on the carbonyl oxygen of the reducing sugar. The initial disaccharide was irradiated with a separate CO₂ laser at 10.6 μm, the *m/z* 179 ion isolated, and its photodissociation (mass spectrum) was recorded as a function of wavelength of the free-electron laser. Plots represent the sum of product ions derived from the *m/z* 179 ion isolated from (blue) ¹⁸O-labeled α-D-Glc*p*-(1→2)-D-Glc and (green) ¹⁸O-labeled β-D-Glc*p*-(1→2)-D-Glc.

dissociate the ¹⁸O-labeled disaccharide (*m/z* 343), giving rise to the *m/z* 179 product ion derived from the non-reducing sugar. The isolated monosaccharide ion was then irradiated using the variable-wavelength free-electron laser source. The evidence for the open-chain form of the monosaccharide derived from either anomeric linkage explains why no information about the anomeric configuration of an unknown disaccharide can be garnered from its monosaccharide product ion (at least, in the negative-ion mode). Evidently, the equilibration of monosaccharides proceeds through the open-chain form at a rate rapid enough to prevent acquisition of independent spectra of either the α or β forms. Considering that the disaccharide ions must reach high vibrational energies for unimolecular dissociation to occur, it is entirely possible that the configurational equilibration rates between forms (Scheme 2) might be much more rapid than those observed in aqueous solution.[29,31,34]

2.4. Theoretical calculations of alkoxy locations and proton transfer for the open-chain alkoxy anions of D-glucose

Using D-glucose as an example, calculations were performed on acyclic and cyclic anionic configurations to assess whether alkoxy groups could potentially reside at different positions and whether intramolecular proton transfer from hydroxyl groups to alkoxy anions was theoretically feasible. For the open-chain configurations having an alkoxy group located independently on O-2 to O-6, their minimum-energy conformations, infrared spectra, and relative enthalpies and free energies were calculated (Fig. 8). It should be pointed out that the minimum free-energy structure arrived at starting with the alkoxy at O-6 corresponded to the

stretch (near 1710 cm⁻¹), indicating that the open-chain configuration of the glucose anion was present to a similar extent, regardless of initial anomeric configuration. A CO₂ laser was used to first

Figure 8. Theoretical calculated minimum-energy conformations, infrared absorption spectra, and overall relative energies for open-chain charge configurations of D-glucose having alkoxy anions at different positions. Shown are ball-and-stick models for the calculated minimum-energy conformation of each charge state, their calculated infrared spectra, calculated relative enthalpies and free energies for the open-chain forms of: (A) the 2-alkoxy anion, (B) the 3-alkoxy anion, (C) the 4-alkoxy anion, (D) the 5-alkoxy anion. Calculations used the program GAUSSIAN03 as discussed in Section 3.

structure having the alkoxy at O-5 via proton transfer (Fig. 8D), so only four stable structures were found. The minimum free-energy conformations that were arrived at (ball-and-stick models, Fig. 8A–D) showed extensive hydrogen-bonding networks. For the O-2 alkoxy anion, for example, OH-3 and OH-4 were hydrogen bonded to the O-2 oxygen, the OH-5 to the OH-4 oxygen and the OH-6 to the OH-5 oxygen. In all stable structures there were two local hydroxyl groups that participated in hydrogen bonding to adjacent alkoxy anions. For the O-3 alkoxy anion, these were OH-2 and OH-4, for the O-4 alkoxy anion, OH-3 and OH-5, and for the O-5 alkoxy anion, OH-4 and OH-6. It is worth noting that the minimum-energy O-2 alkoxy conformation had the lowest relative free energy but that other charge locations were similar enough in free energy to

be significantly populated, provided that proton transfer was possible. Moreover, it would be anticipated that for each alkoxy charge location, rotation about sigma bonds would result in a series of higher energy bond-rotated structures that could also be populated to significant extents, depending on their overall relative free energies.

Importantly, the carbonyl stretching bands that were calculated for the alkoxy positional variants were not identical but ranged from 1700 to 1730 cm^{-1} (Fig. 8). This indicates that, depending on the populations of different alkoxy charge locations, the width of the overall carbonyl absorption peak might be significantly larger than that observed for any single structure, which was observed experimentally. It is also relevant to point out that IRMPD

typically results from absorption of tens to hundreds of IR photons. Well below the internal energies required for multiple-photon dissociation, even prior to the absorption of the very first photon, the open-chain form must be present; otherwise no absorption can occur at frequencies in the carbonyl stretch region.

Mechanistic considerations (Scheme 2) have suggested[7,13,15] that opening of the sugar ring initially proceeds via charge transfer from an O-1 alkoxy group in the cyclic state to an O-5 alkoxy group in the open-chain form. If so, then two conditions should be met. First, the O-1 alkoxy anion structure should be populated. Calculations performed on the cyclic (α-pyranose) anion indeed indicate that the anomeric alkoxy site was favored. Free energies were calculated for the five possible alkoxy anions of the cyclic configurations set relative to the lowest energy open-chain configuration (O-2 alkoxy at 0.0 kcal/mol). They were for position O-1, 4.7 kcal/mol; for position O-2, 9.3 kcal/mol; for position O-3, 10.1 kcal/mol; and for position O-4, 8.1 kcal/mol. The minimum free-energy structure for the 6-alkoxy location optimized to the same structure having the alkoxy at position O-4. These calculations indicated that the free-energy differences between the lowest energy open-chain and cyclic α-pyranose anionic forms were low, and that for the cyclic form the anion containing the O-1 alkoxy group was indeed a preferred and populated structure. Second, if the O-5 alkoxy group is the initially populated charge location upon opening of the sugar ring, then that anionic structure should be of relatively low free energy, and it may be capable, through proton transfers, of distributing charge to other alkoxy locations, resulting in positional anionic variants having low free energies. The O-5 alkoxy form (7.9 kcal/mol, Fig. 8) was of low enough free energy to be appreciably populated, and other open-chain alkoxy locations (the 2, 3 and 4 sites) had even lower calculated free energies. Provided that proton transfers were energetically feasible between hydroxyl and alkoxy groups, these other alkoxy charge sites could be predominant forms in the open-chain configuration. To evaluate this, two transition states were evaluated where a proton was positioned midway between two oxygens at adjacent positions along open-chain configurations, where the negative charge was delocalized. Values found were for an O-4:H:O-5 anionic transition state, 8.6 kcal/mol, and for an O3:H:O4 anionic transition state, 6.1 kcal/mol, calculated for each of their minimum-energy conformations. These calculations indicate that the barriers to proton transfer along an open-chain anion are not large; thus an ensemble of open-chain structures having alkoxy groups at different positions appears feasible.

Finally, it is noted that the recorded spectra show absorptions in the region between 1500 and 1650 cm^{-1} (Figs. 2–5). As shown in Figure 8A, a calculated absorption band was also observed in this region for one charge variant at O-2 having a shifted OH-4 bend frequency. Possibly other higher energy conformers may account for the absorption that was observed experimentally in this region for all the sugar anions (Figs. 2–5), because calculations for all the charge variants of the cyclic configurations in their minimum-energy geometries did not show a calculated absorption band above 1500 cm^{-1}.

2.5. Considerations in comparing gas-phase equilibria in a vacuum to those in solution: solvation effects on monosaccharide anion interconversion rates

Solvation effects are frequently a concern when comparing physical measurements of molecules in solution to measurements performed in vacuo or to theoretical calculations of isolated structures. In aqueous solution, interconversion rates between the structures shown in Scheme 1 are pH dependent, as evaluated by mutarotation studies.[34,58] At a time when the minor forms in solution were not established, the interconversion rates for the

major pyranose forms of glucose at 20 °C could be expressed through an equation, $k_1 + k_2 = 0.0060 + 0.18[H^+] + 16,000[OH^-]$, where k_1 represents the rate constant for the conversion from the α to β form and k_2 represents the rate constant for conversion from β to α.[34,59] Isbell and Wade[58] in an excellent paper summarized a great body of experimental work up to 1967 and described possible mechanisms that were 'water catalyzed' (the first term of 0.0060 in the above equation), 'acid catalyzed' (the second term) or 'base catalyzed' (the third term). Water-catalyzed mechanisms have been the topic of many studies and have generated some controversy, with possible 1–4 water molecules invoked as participatory in multiple mechanisms of ring opening in water or water-aprotic solvent mixtures.[58,60–62] More recently through a series of experiments involving isotope effects among others, it was concluded that only one water molecule needs to participate and that it could not bridge the OH-1 and the ring oxygen.[62] A transition state was proposed where O-1 is mostly deprotonated. For the acid-catalyzed reaction at low pH, it has been suggested that ring opening is accelerated through a different mechanism (and thus transition state) involving protonation of the ring oxygen via intermediary structures involving strong or weak acids or the hydronium ion.[58] Note, however, that the coefficient associated with the concentration of hydroxide is much larger in the third term of the equation. Already at pH 7, a significant component of 0.0016 in that term contributes to a partially base-catalyzed interconversion rate via a separate mechanism.[58] At pH 9 or above this term becomes highly predominant (0.16 at pH 9). Very relevant to the results reported here, it was proposed at high pH that a mechanism involving deprotonation at OH-1 as a first step is operational, resulting in the anionic monosaccharide structures shown in Scheme 2 and not necessarily assuming concurrent protonation at the O-5 position from water during ring opening or rapidly thereafter.[58,35,36] Our studies here indicate that water involvement in the protonation of the ring oxygen need not occur as a *mandatory* participatory event for ring opening of sugar anions, because the carbonyl group of the anions was observed in the gas phase in vacuo independent of any solvent.

Regarding comparative rates of interconversion between the different configurations of the sugar anions in the gas phase or in aqueous solution, as mentioned, ^{13}C NMR studies of glucose anions in aqueous solution at high pH (up to 13.7)[35,36] with complete assignment of all observable signals, showed only two forms, the α and β pyranoses, indicating significantly slower interconversion than the NMR time frame (about 1–2 s). Very low quantities of the other forms shown in Scheme 1 might have been present as anionic species, but were either negligible or not observed. Our studies here indicate significantly higher amounts of the open-chain forms of the sugar anions in the gas phase and much higher interconversion rates. This, in part, could be due to differences in overall thermal energies of the ions in the gas phase as compared to aqueous solution, but the differences could also quite feasibly result from solvation effects. For example, it is possible that water might have an inhibitory effect at high pH on ring opening as compared to the anions in vacuo. Hydrogen bonding of water to the O-1 alkoxy charge of the cyclic forms might inhibit electron density from entering the carbonyl double bond during the shift of C-1 from sp^3 to sp^2 hybridization that must occur somewhere along the reaction coordinate during ring opening. Also, as compared to the sugar ions in the gas phase, their aqueous solutions at high pH are complicated by the presence of counterions (either Na$^+$ or K$^+$ in previous NMR studies)[35,36] that would interact strongly with the O-1 alkoxy negative charge and could also coordinate with lone-pair electrons from the oxygens of the sugar hydroxyl groups. Furthermore, the entropic contributions of the sugar anions and the solvent to the overall free energies of the different configurations in solution are difficult to assess.

Lewis and Schramm[35] also provided evidence in aqueous solution at high pH that the cyclic anionic forms of glucose can be deprotonated to lesser extents at positions other than OH-1. This was based on tritium isotope effects at different positions on the molecule using anion-exchange chromatography at high pH, ^{13}C NMR spectroscopy at high pH, and high level quantum chemical calculations. That the OH-1 of reducing monosaccharides need not be the only site of deprotonation in solution is also borne out in ^{13}C NMR studies of sucrose at high pH, where deprotonation occurred at different hydroxyl locations even though an anomeric OH-1 is absent.[63]

2.6. Further discussion and caveats

Based on the above results, open-chain configurations were observed for all eight aldohexoses isolated as anions in the gas phase. Three possible reasons may account for the different wavelength maxima of their product ions observed in the carbonyl stretch region. (1) As mentioned above, an ensemble of different charge sites may be present, with alkoxy anions potentially located at any position other than C-1 or C-6 for the open-chain form(s). Each charge variant within the family, for a single sugar, may have preferential dissociation channels, giving rise to the different wavelength maxima observed for individual product ions. (2) Product ions are also susceptible to further dissociation using IRMPD. Some product ions, for example, did not appear to increase in abundance in stepping through the carbonyl stretch region, depending on the aldohexose, which we can only attribute to their increased susceptibility to dissociation relative to the precursor ion itself. Each product ion may also have its own wavelength dependence for dissociation; thus the overall spectrum is the sum of fragmentation events of precursor and product ions. (3) Each ion absorbs infrared photons to some threshold level of internal energy required for dissociation. The extent of heating above the threshold can result in dissociation channels, or pathways, becoming available that would not be available at or slightly above the dissociation threshold. Therefore, depending on the *rate* of energy absorption at specific wavelengths, some dissociation channels may be favored, or made available, both for precursor or product ions. Nonetheless, regardless of whether the precursor or product ions of an aldohexose undergo differential dissociation, it is clear that the different wavelength optima of the product ions observed for the different hexoses must be attributed to the stereochemical difference(s) among them.

In addition to the complexities in interpretation of the wavelength-dependence discussed above, it is worth pointing out some caveats of reproducibility using infrared photodissociation in general using FTICR instruments. Commercially available instruments use a CO_2 laser with a fixed wavelength of 10.6 μm. Product mass spectra are dependent on laser alignment, power and irradiation time. While good mass spectral reproducibility can be maintained over short periods (a few weeks), the stability of laser outputs over long time periods must be checked with a power meter and adjusted in combination with the duration of irradiation to obtain a similar net photon input. Also, lasers that are kept locked in position near the input window of the mass spectrometer do not require frequent realignment and hence tend to give more reproducible results. The laser pulse structure of the FELIX free-electron laser is quite different from that of cw or pulsed CO_2 lasers or optical parametric oscillator (OPO) lasers. FELIX irradiation pulses are generated as a sequence of short micropulses bunched into groups of macropulses, with macropulses occurring at regular time intervals of 200 ms in this study.[64] The intervals between micropulses and macropulses allow time for absorbed photons to equilibrate through intramolecular vibrational redistribution and to some extent, through emission. Other FTICR instruments having independent

laser sources would be expected to generate spectra that could be somewhat different in ion ratios than the figures presented herein. However, differences in spectra using photodissociation with other instruments is not unlike differences obtained with similar instruments using CID. With an ion trap, for example, changing the collision energy, the q factor or the collision time will dramatically affect the product mass spectrum, and different types of traps also result in minor but reproducible differences in spectra.[22] Nevertheless, the scanning capability of the free-electron laser has enabled some important aspects of infrared absorption and photodissociation at the carbonyl frequency to be studied with aldohexoses and is worthy of further investigation with free-standing lasers or other sources that cover the 1650–1750 cm^{-1} wavelength range.

3. Experimental

Infrared photodissociation experiments were carried out using a Fourier-transform ion cyclotron resonance mass spectrometer using mass-selected anions of the monosaccharides (m/z 179). Ions were irradiated with macropulses from the *F*ree *E*lectron *L*aser for *I*nfrared e*X*periments (FELIX) located at the FOM Institute for Plasma Physics Rijnhuizen, Nieuwegein, The Netherlands.[64] The laser generates a series of micropulses of picosecond duration separated by 1 ns, based on the timing of electron bunches used to generate the IR light. A whole pulse train of micropulses comprises a 'macropulse' which is ≈5 μs in length. Finally, a series of macropulses (30 macropulses over 6 s, each containing about 35 mJ/pulse) was used to dissociate the anions. FELIX generates pulses with a full width at half-maximum of 0.5% of the central linewidth (i.e., about 5 cm^{-1} at 1000 cm^{-1}). The laser wavelength was varied between 5.5 and 11.4 μm (880–1820 cm^{-1}) and mass spectra were recorded at each of 150–170 wavelengths stepped in 0.03–0.05 μm increments. Variation of the precursor ion abundance and individual product ions or the sum of product ions was plotted as the percentage of total ions, whereby the presence of characteristic functional groups and other aspects of structure can be assessed as a function of IR wavelength.[46,65,66] Plots were mildly smoothed using a 3-point moving average.

Ionization was carried out using a commercial electrospray-ionization source (Micromass, Manchester, UK). Ions were accumulated in a linear storage hexapole for the duration of the previous FTICR sequence (about 7 s) and then pulse-extracted. They passed through a quadrupole deflector (ABB Extrel) and an octopole guide, thence into the ICR cell.[66]

All aldohexoses were of the D-form. Glucose, galactose and mannose were purchased from Sigma–Aldrich Chemical Co. Allose, gulose, altrose and talose were from MP Biomedicals. Idose was from Omicron Biochemicals. The disaccharides, sophorose (β-D-Glc*p*-(1→2)-D-Glc) and kojibiose (α-D-Glc*p*-(1→2)-D-Glc) were purchased from Serva Biochemicals and Koch–Light Laboratories, respectively. Sugars were prepared at 1 mM in a solution of 95:5–98:2 MeOH/water (vol/vol) containing 1 mM NaOH. The freshly prepared solutions were introduced immediately into the mass spectrometer using an electrospray-ionization source, and sprayed continuously for a period of about 90 min during acquisition of spectra stepped over multiple wavelengths. Independent nuclear magnetic resonance spectroscopy experiments of solutions of glucose and galactose in 90:10 CD_3OD/D_2O containing 1 mM NaOH were carried out at 500 MHz at the University of Colorado-Denver, Anschutz Medical Campus. Solutions were followed over time to evaluate whether these sugars enolized[33,67] significantly under these conditions. No change was observed over a two-hour period, although after 4 days, evidence was seen for enolization. As the 1 mM NaOH was required for ionization using the source in the Netherlands, all solutions were freshly prepared and analyzed immediately. The NaOH was not required for adequate

generation of aldohexose anions on another instrument (a Thermo-Finnigan LTQ-FTICR Ultra) located at the University of Colorado-Denver, where the front-end linear ion trap greatly improved sensitivity prior to introduction into the FTICR.

Labeling the reducing end of the disaccharides with ^{18}O was carried out as previously described.[14,15] Disaccharides (1 mg) were dissolved in $H_2{}^{18}O$ (Cambridge Isotopes, 100 µL) for 4 days, and stored frozen. Just prior to use, this solution was diluted to 1 mM in MeOH containing 1 mM NaOH, and the ^{18}O-labeled disaccharide anion having m/z 343 was isolated and subsequently irradiated.

Theoretical calculations of the anionic structures and infrared spectra for open-chain and cyclic configurations of D-glucose utilized the program GAUSSIAN03,[68] carried out to the same level of theory for each anionic and transition state variant. Minimum-energy structures were initially geometry optimized with the B3LYP/6-311G++(d,p) functional and basis set combination, then subsequently single-point energy calculated at that geometry using MP2/6-311G++(d,p). Vibrational frequencies were scaled by 0.965. Intramolecular hydrogen bonding differed among the anionic variants having the alkoxy group at different positions. Calculations were carried out for alkoxy anions located from O-2 to O-6 for the acyclic configurations, and from O-1 to O-4 and O-6 for the cyclic forms. Calculations were also carried out for two transition states in open-chain configurations where the proton from one hydroxyl group having an adjacent alkoxy site was positioned midway between the oxygens, thereby delocalizing the negative charge. Transition states were calculated with either a proton shared between the O-3 and O-4 or between the O-4 and O-5 positions.

4. Summary and conclusions

Irradiation of the anions of aldohexoses in the gas phase using infrared wavelengths in the carbonyl stretch region showed a relatively large absorbance peak as measured by photodissociation of the ions, indicating a significant proportion of the open-chain form. Due to differences in dissociation patterns unique to each aldohexose, mass spectra displayed marked changes in product ion ratios over the spectral region covering carbonyl stretch wavelengths. Wavelength maxima for specific product ion abundances varied over this region, which included different product ions from the same sugar as well as the same product ions in comparing different sugars. Theoretical calculations indicate that an ensemble of open-chain charge locations is possible having alkoxy anions at different positions. Photodissociation in the carbonyl stretch region enabled the stereochemistry of aldohexoses to be differentiated. Further investigation is warranted with other FTICR instruments and sources covering the 1650–1750 cm^{-1} wavelength range. Experiments on sugar anions in the gas phase also shed light on mechanisms invoking the participation of water in interconversions of sugar configurations under aqueous basic conditions, because opening of the sugar rings as anions in vacuo is an intrinsic property of the ions independent of solvent.

Acknowledgments

References

1. Paul, W.; Reinhard, H. P.; von Zahn, U. Z. Phys. **1958**, 152, 143–182.
2. Hager, J. W. Rapid Commun. Mass Spectrom. **2002**, 16, 512–526.
3. Yost, R. A.; Enke, C. G.; McGilvery, D. C.; Smith, D. L.; Morrison, J. D. Int. J. Mass Spectrom. Ion Phys. **1979**, 30, 127–136.
4. Stephens, W. E. Phys. Rev. **1946**, 69, 691. meeting abstract J1.
5. Yergey, A. L.; Coorssen, J. R.; Backlund, P. S.; Blank, P. S.; Humphrey, G. A.; Zimmerberg, J.; Campbell, J. M.; Vestal, M. L. J. Am. Soc. Mass Spectrom. **2002**, 13, 784–791.
6. Marshall, A. G. Int. J. Mass Spectrom. **2000**, 200, 331–356.
7. Dallinga, J. W.; Heerma, W. Biol. Mass Spectrom. **1991**, 20, 215–231.
8. Ballistreri, A.; Montaudo, G.; Garozzo, D.; Giuffrida, M.; Impallomeni, G. Rapid Commun. Mass Spectrom. **1989**, 3, 302–304.
9. Garozzo, D.; Giuffrida, M.; Impallomeni, G.; Ballistreri, A.; Montaudo, G. Anal. Chem. **1990**, 62, 279–286.
10. Garozzo, D.; Impallomeni, G.; Spina, E.; Green, B. N.; Hutton, T. Carbohydr. Res. **1991**, 221, 253–257.
11. Carroll, J. A.; Ngoka, L.; Beggs, C. G.; Lebrilla, C. B. Anal. Chem. **1993**, 65, 1582–1587.
12. Mulroney, B.; Traeger, J. C.; Stone, B. A. J. Mass Spectrom. **1995**, 30, 1277–1283.
13. Mulroney, B.; Peel, J. B.; Traeger, J. C. J. Mass Spectrom. **1999**, 34, 856–871.
14. Fang, T. T.; Zirrolli, J.; Bendiak, B. Carbohydr. Res. **2007**, 342, 217–235.
15. Fang, T. T.; Bendiak, B. J. Am. Chem. Soc. **2007**, 129, 9721–9736.
16. Zhou, Z.; Ogden, S.; Leary, J. A. J. Org. Chem. **1990**, 55, 5444–5446.
17. Hofmeister, G. E.; Zhou, Z.; Leary, J. A. J. Am. Chem. Soc. **1991**, 113, 5964–5970.
18. Dongre, A. R.; Wysocki, V. H. Org. Mass Spectrom. **1994**, 29, 700–702.
19. Asam, M. R.; Glish, G. L. J. Am. Soc. Mass Spectrom. **1997**, 8, 987–995.
20. Polfer, N. C.; Valle, J. J.; Moore, D. T.; Oomens, J.; Eyler, J. R.; Bendiak, B. Anal. Chem. **2006**, 78, 670–679.
21. Simoes, J.; Domingues, P.; Reis, A.; Nunes, F. M.; Coimbra, M. A.; Domingues, M. R. M. Anal. Chem. **2007**, 79, 5896–5905.
22. Bendiak, B.; Fang, T. T. Carbohydr. Res. **2010**, 345, 2390–2400.
23. Salpin, J.-Y.; Tortajada, J. J. Mass Spectrom. **2002**, 37, 379–388.
24. Zhu, X.; Sato, T. Rapid Commun. Mass Spectrom. **2007**, 21, 191–198.
25. Dallinga, J. W.; Heerma, W. Biomed. Environ. Mass Spectrom. **1989**, 18, 363–372.
26. Carroll, J. A.; Willard, D.; Lebrilla, C. B. Anal. Chim. Acta **1995**, 307, 431–447.
27. Spengler, B.; Dolce, J. W.; Cotter, R. J. Anal. Chem. **1990**, 62, 1731–1737.
28. Maple, S. R.; Allerhand, A. J. Am. Chem. Soc. **1987**, 109, 3168–3169.
29. Los, J. M.; Simpson, L. B.; Wiesner, K. J. Am. Chem. Soc. **1956**, 78, 1564–1568.
30. Hayward, L. D.; Angyal, S. J. Carbohydr. Res. **1977**, 53, 13–20.
31. Dworkin, J. P.; Miller, S. L. Carbohydr. Res. **2000**, 329, 359–365.
32. Fischer, E. Ber. Dtsch. Chem. Ges. **1884**, 17, 579–584.
33. Lobry de Bruyn, M. M. C. A.; Alberda van Ekenstein, W. Recl. Trav. Chim. Pays-Bas **1895**, 14, 203–216.
34. Pigman, W.; Anet, E. F. L. J. In Pigman, W., Horton, D., Eds., 2nd ed.; The Carbohydrates, Chemistry and Biochemistry; Academic Press: New York, 1972; Vol. 1A, pp 165–194.
35. Lewis, B. E.; Schramm, V. L. J. Am. Chem. Soc. **2003**, 125, 7872–7877.
36. de Wit, G.; Kieboom, A. P. G.; van Bekkum, H. Recl. Trav. Chim. Pays-Bas **1979**, 98, 355–361.
37. Kim, M. S.; McLafferty, F. W. J. Am. Chem. Soc. **1978**, 100, 3279–3282.
38. Stefan, S.; Eyler, J. R. Anal. Chem. **2009**, 81, 1224–1227.
39. Dunbar, R. C. In Gas Phase Ion Chemistry; Bowers, M. T., Ed.; Academic Press: New York, 1979; Vol. 2, pp 180–220.
40. Freiser, B. S.; Beauchamp, J. L. J. Am. Chem. Soc. **1974**, 96, 6260–6266.
41. Eyler, J. R. J. Am. Chem. Soc. **1976**, 98, 6831–6834.
42. Woodin, R. L.; Bomse, D. S.; Beauchamp, J. L. J. Am. Chem. Soc. **1978**, 100, 3248–3250.
43. Baykut, G.; Watson, C. H.; Weller, R. R.; Eyler, J. R. J. Am. Chem. Soc. **1985**, 107, 8036–8042.
44. Devakumar, A.; Thompson, M. S.; Reilly, J. P. Rapid Commun. Mass Spectrom. **2005**, 19, 2313–2320.
45. Racaud, A.; Antoine, R.; Joly, L.; Mesplet, N.; Dugourd, P.; Lemoine, J. J. Am. Soc. Mass Spectrom. **2009**, 20, 1645–1651.
46. Eyler, J. R. Mass Spectrom. Rev. **2009**, 28, 448–467.
47. Dela Cruz, J. M.; Lozovoy, V. V.; Dantus, M. J. Mass Spectrom. **2007**, 42, 178–186.
48. Pastirk, I.; Zhu, X.; Lozovoy, V. V.; Dantus, M. Appl. Opt. **2007**, 46, 4041–4045.
49. Zhang, J.; Schubothe, K.; Li, B.; Russell, S.; Lebrilla, C. B. Anal. Chem. **2005**, 77, 208–214.
50. Kuhn, L. P. Anal. Chem. **1950**, 22, 276–283.
51. Tipson, R. S.; Parker, F. S. In Pigman, W., Horton, D., Eds., 2nd ed.; The Carbohydrates, Chemistry and Biochemistry; Academic Press: New York, 1980; Vol. 1B, pp 1394–1436.
52. Mathlouthi, M.; Koenig, J. L. Adv. Carbohydr. Chem. Biochem. **1986**, 44, 7–89.
53. Cagmat, E. B.; Szczepanski, J.; Pearson, W. L.; Powell, D. H.; Eyler, J. R.; Polfer, N. C. Phys. Chem. Chem. Phys. **2010**, 12, 3474–3479.
54. Oomens, J.; Moore, D. T.; Meijer, G.; von Helden, G. Phys. Chem. Chem. Phys. **2004**, 6, 710–718.
55. von Helden, G.; van Heijnsbergen, D.; Meijer, G. J. Phys. Chem. A **2003**, 107, 1671–1688.
56. Oomens, J.; Sartakov, B. G.; Meijer, G.; von Helden, G. Int. J. Mass Spectrom. **2006**, 254, 1–9.
57. Swenson, C. A.; Barker, R. Biochemistry **1971**, 10, 3151–3154.
58. Isbell, H. S.; Wade, C. W. R. J. Res. Natl. Bur. Stand. Sect. A **1967**, 71, 137–148.

59. Isbell, H. S.; Pigman, W. *J. Res. Natl. Bur. Stand.* **1938**, *20*, 773–798.
60. Kjaer, A. M.; Sorensen, P. E.; Ulstrup, J. *J. Chem. Soc., Perkin Trans. 2* **1978**, 51–59.
61. Yamabe, S.; Ishikawa, T. *J. Org. Chem.* **1999**, *64*, 4519–4524.
62. Lewis, B. E.; Choytun, N.; Schramm, V. L.; Bennet, A. J. *J. Am. Chem. Soc.* **2006**, *128*, 5049–5058.
63. Popov, K. I.; Sultanova, N.; Ronkkomaki, H.; Hannu-Kuure, M.; Jalonen, J.; Lajunen, L. H. J.; Bugaenko, I. F.; Tuzhilkin, V. I. *Food Chem.* **2006**, *96*, 248–253.
64. Oepts, D.; van der Meer, A. F. G.; van Amersfoort, P. W. *Infrared Phys. Technol.* **1995**, *36*, 297–308.
65. Oomens, J.; Young, S.; Molesworth, S.; van Stipdonk, M. *J. Am. Soc. Mass Spectrom.* **2009**, *20*, 334–339.
66. Polfer, N. C.; Oomens, J. *Phys. Chem. Chem. Phys.* **2007**, *9*, 3804–3817.
67. Whistler, R. L.; BeMiller, J. N. *Adv. Carbohydr. Chem.* **1958**, *13*, 289–329.
68. Frisch, M. J.; Trucks, G. W.; Schlegel, H. B.; Scuseria, G. E.; Robb, M. A.; Cheeseman, J. R.; Montgomery, J. A., Jr.; Vreven, T.; Kudin, K. N.; Burant, J. C.; Millam, J. M.; Iyengar, S. S.; Tomasi, J.; Barone, V.; Mennucci, B.; Cossi, M.; Scalmani, G.; Rega, N.; Petersson, G. A.; Nakatsuji, H.; Hada, M.; Ehara, M.; Toyota, K.; Fukuda, R.; Hasegawa, J.; Ishida, M.; Nakajima, T.; Honda, Y.; Kitao, O.; Nakai, H.; Klene, M.; Li, X.; Knox, J. E.; Hratchian, H. P.; Cross, J. B.; Bakken, V.; Adamo, C.; Jaramillo, J.; Gomperts, R.; Stratmann, R. E.; Yazyev, O.; Austin, A. J.; Cammi, R.; Pomelli, C.; Ochterski, J. W.; Ayala, P. Y.; Morokuma, K.; Voth, G. A.; Salvador, P.; Dannenberg, J. J.; Zakrzewski, V. G.; Dapprich, S.; Daniels, A. D.; Strain, M. C.; Farkas, O.; Malick, D. K.; Rabuck, A. D.; Raghavachari, K.; Foresman, J. B.; Ortiz, J. V.; Cui, Q.; Baboul, A. G.; Clifford, S.; Cioslowski, J.; Stefanov, B. B.; Liu, G.; Liashenko, A.; Piskorz, P.; Komaromi, I.; Martin, R. L.; Fox, D. J.; Keith, T.; Al-Laham, M. A.; Peng, C. Y.; Nanayakkara, A.; Challacombe, M.; Gill, P. M. W.; Johnson, B.; Chen, W.; Wong, M. W.; Gonzalez, C.; Pople, J. A. GAUSSIAN *03, Revision E.01*; Gaussian, Inc.: Wallingford CT, 2004.